Journal of
Micro/Nanolithography, MEMS, and MOEMS

SPIEDigitalLibrary.org/jm3

Mesoscale modeling: a study of particle generation and line-edge roughness

Siddharth Chauhan
Mark Somervell
Michael Carcasi
Steven Scheer
Roger T. Bonnecaze
Chris A. Mack
C. Grant Willson

SPIE

Mesoscale modeling: a study of particle generation and line-edge roughness

Siddharth Chauhan,[a] Mark Somervell,[b] Michael Carcasi,[b] Steven Scheer,[b] Roger T. Bonnecaze,[a] Chris A. Mack,[c] and C. Grant Willson[a,*]
[a]The University of Texas at Austin, Department of Chemical Engineering, Austin, Texas 78712
[b]Tokyo Electron America Ltd., 2400 Grove Boulevard, Austin, Texas 78741
[c]Lithoguru.com, 1605 Watchhill Road, Austin, Texas 78703

Abstract. A lattice-type Monte Carlo–based mesoscale model and simulation of the lithography process have been adapted to study the insoluble particle generation that arises from statistically improbable events. These events occur when there is a connected pathway of soluble material that envelops a volume of insoluble material due to fluctuations in the deprotection profile. The simulation shows that development erodes the insoluble material into the developer stream and produces a cavity on the line edge that can be far larger than a single polymer molecule. The insoluble particles can coalesce to form aggregates that deposit on the wafer surface. The effect of the resist formulation, exposure, postexposure bake, and development variables on particle generation was analyzed in both low- and high-frequency domains. It is suggested that different mechanisms are dominant for the formation of line-edge roughness (LER) at different frequencies. The simulations were used to assess the commonly proposed measures to reduce LER such as the use of low molecular weight polymers, addition of quenchers, varying acid diffusion length, etc. The simulation can be used to help set process variables to minimize the extent of particle generation and LER. *© 2014 Society of Photo-Optical Instrumentation Engineers (SPIE)*
[DOI: 10.1117/1.JMM.13.1.013012]

Keywords: mesoscale modeling; particle generation; line-edge roughness; correlation length; polymer dissolution.

Paper 13105P received Jun. 27, 2013; revised manuscript received Nov. 6, 2013; accepted for publication Feb. 6, 2014; published online Mar. 12, 2014.

1 Introduction

Defectivity has always been a key concern for the semiconductor industry. Because they lead to lost yield and therefore lost revenue, defects are constantly investigated in every manufacturing facility in the world. Although lithography processes are very clean, they are not perfect, and all have some level of defectivity. One important class of lithographic defects is "postdevelop defects" that are generated during development of the photoresist. It has been proposed that these insoluble residues are generated by an erosion event that occurs when there is, generated by chance, a connected pathway of soluble material that envelops or surrounds an insoluble volume.[1,2] Such residues or particles are inherently insoluble photoresist materials that would have a tendency to redeposit on the wafer or the tools. Any drop in the pH of the solution, like that which occurs during the rinse step, would aggravate the problem by further reducing the solubility of the particles already suspended in the solution. These statistical excursions of the development path during photoresist dissolution can produce a cavity on the line edge that is far larger than the volume of a single polymer molecule.

A different but closely related problem in manufacturing is line-edge roughness (LER). The International Technology Roadmap for Semiconductors has outlined LER as one of the major challenges ahead, as the critical dimension (CD) on the integrated circuit (IC) chip is approaching molecular dimensions.[3] For example, LER generates a random variation in gate length (CD). These variations in CD affect the device performance by introducing variations in threshold voltage and on-off current. The morphology of a line edge depends on the length scale of observation.[4] Therefore, in the recent past, the characterization of LER has been based not only on the rms value σ (standard deviation of the line edge), but also the spatial aspects of LER based on parameters including correlation length and roughness exponent. Ma et al. evaluated the impact of the individual parameters on CD variation from a statistical prospective.[5] They found that smaller gate widths, larger correlation lengths, and smoother local edge roughness (larger roughness exponent) produce larger CD variations. The low-frequency LER produces transistor gate length variations leading to current leakage and IC timing issues, while the high-frequency LER affects dopant concentration profiles and interconnect wire resistance.[3]

Simulation studies have proven to be a time- and cost-effective approach to solving several engineering problems. Lithographic simulation and Monte Carlo techniques are now being used throughout the industry to predict CD error budgets, process windows, and other important lithographic parameters. However, the subject of defectivity has largely remained untouched by these simulations. Defectivity is a stochastic process, and Monte Carlo simulations inherently make use of stochastics, so an attempt has been made to exploit Monte Carlo techniques to simulate particle generation during the photoresist dissolution step. These simulations also provide valuable information about the fundamental causes of LER and aid in studying the convoluted variables individually, which is not feasible experimentally.

Mesoscale modeling is a promising simulation approach based on molecular-level interactions and capable of

*Address all correspondence to: C. Grant Willson, E-mail: willson@che.utexas.edu

0091-3286/2014/$25.00 © 2014 SPIE

predicting stochastic responses such as LER. Our group has developed a three-dimensional (3-D) mesoscale model that enables simulation of the lithographic processes including spin-coating, postapply bake, exposure, postexposure bake (PEB), and dissolution. The stochastic variations in the deprotection profile produced during PEB are captured by simulating the reactive transport processes based on a new proposed transient acid diffusion mechanism.[6] A mesoscale, dynamic Monte Carlo model for photoresist dissolution based on the molecular-level interactions between distinct components of the resist and the developer has been developed and used in the current study.[7] These recent improvements in our simulator have enabled detection of volumes of insoluble material eroded into the developer near the line edge during development. These advancements have also provided access to valuable information about the relative contributions of different lithographic steps to LER and thereby insight into the fundamental causes of LER.

2 Mesoscale Modeling

The present simulation work relies on mesoscale modeling[1] of a model photoresist comprising copolymers of *p*-hydroxystyrene and *t*-butyloxycarbonyloxystyrene. A 3-D cubic lattice structure was created to simulate the photoresist film. Each cell in the lattice is assigned either as a monomer (where a string of connected monomer cells represents a polymer chain), photoacid generator (PAG), quencher, or a void. A completely random configuration is obtained using a Monte Carlo approach with periodicity in the given direction. Next, the most relevant and recently revised simulation modules, namely PEB and dissolution, are briefly described.

2.1 *Postexposure Bake*

Acid diffusion in a chemically amplified resist amplifies the variation in protection level near the interface of the exposed-unexposed region. The roughness in the protection level is believed to be a major contributor to the LER observed after the dissolution step. Needless to say, an accurate acid diffusion model is therefore critical for any LER study. Experimental results have demonstrated a fast acid diffusion for the first ~1 min of the PEB followed by a tremendous slowdown in subsequent acid diffusion rate.[8] The reported diffusivity of acid in pure poly(p-hydroxystyrene) is very small ($<10^{-7}$ cm^2/s) at typical PEB temperature and would result in a mean diffusion length of only ~1 nm. Postnikov proposed a reaction front propagation model to explain the observed acid diffusion behavior.[9] He postulated that the deprotection reaction causes local, transient enhancement of acid diffusivity, which results in high acid diffusion at the reaction front but this enhanced diffusivity lasts only for a very short period of time. The concept of reaction-enhanced diffusivity could be explained for APEX-type 248-nm resists by invoking transient free volume generation during the deprotection reaction as the mechanism for diffusivity enhancement.[1] Clearly, the loss of volatile products such as isobutylene that occurs during PEB could cause a local and transient plasticization of the film and/or could generate a transient and local volume of reduced density. Of course, this low-density condition is short lived because the film collapses to produce the familiar relief image that is observed after the PEB. Unfortunately, this mechanism for the transient enhancement of diffusivity does not apply to methyladamantyl protected 193-nm resists where the by-product of the deprotection reaction is not volatile as it is in APEX-type 248-nm resists.

A different explanation for this phenomenon relies on heat from the exothermic deprotection reaction to elevate the local temperature above the glass transition temperature (T_g) of the polymer, thus enhancing the acid diffusivity in a local region.[6,10] The diffusivity or permeance of a polymer film changes by several orders of magnitude when the local temperature exceeds T_g. As time progresses, the heat generated by the reaction diffuses away from the local region until the local temperature drops below T_g, thus rendering only a transient acid diffusivity enhancement. Any acid molecule that happens to be in a volume of polymer above T_g is able to diffuse rapidly. During this diffusion, if an acid molecule encounters any protected site, it can catalyze another deprotection reaction and it then continues to diffuse. However, if the reaction front has moved forward and there are no reaction sites available, the local matrix will cool below T_g and the acid molecule will diffuse no further. Eventually, all the acid molecules become trapped and the reaction front stops, not because of loss of chemical reactivity, but because the acid catalyst is immobilized.

The temperature profile around the deprotection site was estimated by solving the heat equation in spherical coordinates with an isolated heat source at the center.[11] The local diffusivity was estimated on the basis of the empirical relationship between the temperature and the diffusivity.[8] However, for simplicity, a binary profile for acid diffusion was employed in which the acid is allowed to diffuse only when the local temperature is above the given temperature and below that temperature it is immobile. In order to facilitate the computation, the present model allows an acid molecule to diffuse through and share a lattice site with other resist components. Thus, the excluded volume condition is relaxed, a characteristic which is inherently assumed in continuum models.

2.2 *Photoresist Dissolution*

At the onset of the development simulation step, a developer film is added to the lattice structure with lattice grids extended into the developer film. The dissolution model assumes that the base is readily available for deprotonation at polymer acidic sites and there is no depletion zone. When the aqueous base (developer) comes in contact with the polymer, deprotonation of the ionizable acidic sites causes accumulation of a negative charge at the polymer-developer interface.[12] The charged surface results in the depletion of hydroxide ions near the interface, and an electric double layer is formed. The Poisson–Boltzmann equation and the equilibrium conditions are used to yield the ion concentration at the charged surface and the corresponding fractional surface ionization. Thereafter, the surface is fractionally ionized and the dynamic equilibrium is maintained by considering ionization/deionization step at the polymer–developer interface. Polymer chain motion and chain solvation at the film-developer interface are simulated using the Metropolis algorithm where the probability of a move is based on the energetics of interactions between different species in the polymer and the developer. Mesoscale modeling using this approach not only accounts for the favorable interaction between the ionized part of the polymer and the developer

solution to render the polymer soluble as in the critical ionization model,[13] but also takes into account the chain configuration and the interactions of the nonionized part of the chain with the developer and the polymer film. The interaction parameters for different species in the system were based on experimentally determined interfacial energy values, and the ionized polymer-developer interaction parameter was determined by calibrating the simulated dissolution rate response to polymer molecular weight and developer concentration against measured values.[14,15–17] After the photoresist dissolution is simulated for a given period of time, the rinse step is simulated. The developer is replaced with water, and all of the ionized sites of polymer chains are deionized. The dangling chains are then settled down against the lattice to reach the favored lower energetic state. Finally, a denser film–air interface is attained with roughness at the surface. The roughness is characterized and analyzed in a later section.

3 Insoluble Particle Generation

An aerial image profile produces an acid gradient in the exposed resist film. During the PEB, the acid gradient results in a corresponding gradient in the average protection level (chemical gradient). There is a certain degree of stochastic variation in the average blocking level. Figure 1 shows the average protection level (averaged over $y-z$ plane at any given x) with $\pm\sigma$ variation in the protection level at different y along the $y-z$ plane as a function of x-dimension of a feature. For the sake of argument, assume that the polymer solubility switch occurs at 25% protection level. The protection level to the left of $x=a$ is higher than the solubility threshold and therefore, the resist volume is insoluble. On the other hand, the protection level to the right of $x=b$ is lower than the solubility threshold, implying that everything to the right of $x=b$ is soluble. However, there exists a solubility crossover region with a finite width d between $x=a$ and $x=b$ where part of the resist volume is soluble (protection level lower than threshold limit) while the rest of it is inherently insoluble (protection level above the threshold limit). Solvation of each polymer chain within the soluble volume paves a path that allows the developer to penetrate and interact with the lower chain. If there exists a connected pathway of soluble material that envelopes a volume of insoluble material in the solubility crossover region, development erodes that insoluble material into the developer stream as an insoluble particle. It is worthy to note that this analysis is a simplistic representation of the current problem. Here, variation in protection level in z direction has not been considered. That is, the influence of film absorbance has been neglected. In reality, the possibility of connected pathways and the statistics (size distribution, protection level, etc.) of insoluble particles generated depend on the actual 3-D configuration of resist components and the development mechanism. Therefore 3-D mesoscale models for the PEB and dissolution steps discussed in earlier sections are crucial in this study.

The detection of the particles during a dissolution run is important and requires a suitable search algorithm. The network of chains in contact with the substrate defines the bulk resist film, and any group of chains detached from the resist film but not dissolved yet is considered as a particle. The connectivity between the two chains is determined by a minimum of one direct contact between the chains or indirect contact through a series of chains. A simplistic but computationally expensive approach for particle detection would then be to scan all the chains for connectivity using any standard search algorithm such as the breadth first search algorithm. Actually, the connectivity of only the interfacial chains, i.e., those outer chains that are in direct contact with developer, is the sufficient and necessary condition for no particle generation. The interfacial chains are a small fraction of the total number of chains and therefore considering them only cuts down the search time considerably. The interfacial chains are tracked and updated at each Monte Carlo step and are periodically scanned for their connectivity through interfacial chains. If all interfacial chains are connected then there exists no particle and the particle search ends. When the interfacial chains are not all connected, then all the chains (interfacial as well as bulk chains) must be scanned for their connectivity to identify the particle. This step is computationally expensive but rare and thus the costly redundancy of scanning all the chains each time is avoided. Finally, particle details are recorded and the particle is removed from the lattice structure for the rest of the simulation.

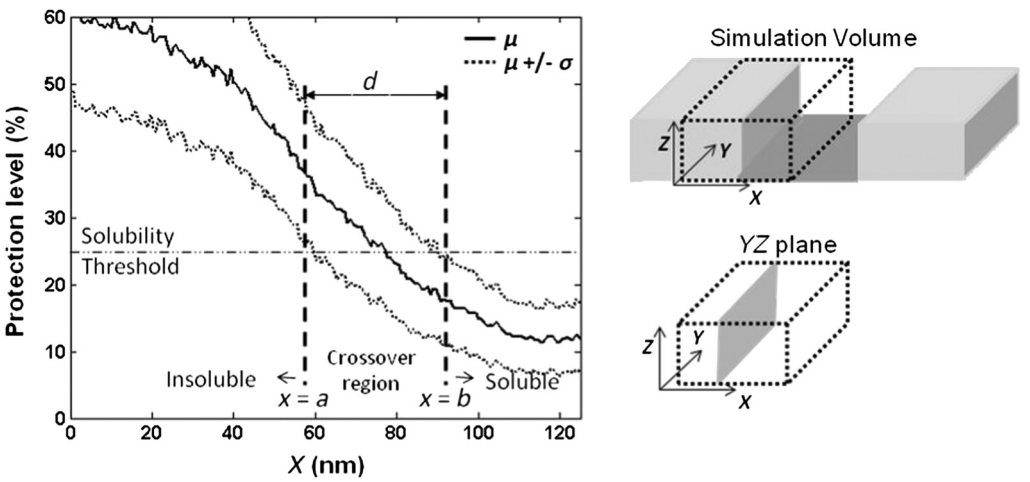

Fig. 1 The average protection level is shown with a solid line (averaged over $y-z$ plane at any given x). The dotted lines show the limits of one standard deviation in the protection level at different y along the $y-z$ plane as a function of the x-dimension.

Once a particle has been generated, it can settle on the tooling, on the wafer, be rinsed away during the rinsing process, or dissolve in developer. Investigating the fate of the particles requires longer tracking and is beyond the scope of the current work. Figure 2(a) shows the size distribution of the particles generated during a photoresist dissolution run based on the typical simulation inputs outlined in the next section. Here, particle size is actually the number of polymer chains in the particle. As expected, there is a large number of small particles and fewer big particles. To give some prospective to the volume, a single chain occupies ~27 nm^3 in the simulation lattice structure. Once a simulation run is over, different statistics can be employed to do a postanalysis of the particle generation study. The total number of particles, average blocking of the particles, the number average size of the particles, and volume percentage of particles generated are shown in Fig. 2(a). For the purposes of this paper, the metric used to quantify particle generation is the volume percentage of the insoluble particles in the total resist volume dissolved. Figure 2(b) shows a snapshot of the dissolution run showing the particles generated.

The following configuration setup is used for the particle generation study: a film of APEX type resist with dimensions of $130 \times 250 \times 100$ nm (half pitch × line length × film thickness) was simulated using a $184 \times 356 \times 144$ lattice structure with periodic boundary conditions only along the line length. The following resist formulation and process conditions, unless otherwise specified, were used in the particle generation study. The resist that was simulated is formulated from a polymer with degree of polymerization of 80, 60% protection level, pKa of 10.25, 5 wt. % PAG loading, and 20% quencher loading (relative to PAG concentration). The exposure conditions involve normalized image log slope (NILS) equals to 2.41, dose to size with Dill C parameter as 0.03 cm^2/mJ, and the image in resist using PROLITH for typical KrF resist. The PEB time and the temperature were 60 s and 90°C, respectively. A development time of 30 s with standard 0.26 N developer concentration was used in the development step. Typical results reported are an average of 10 simulation runs. Next, the parametric study is presented for polymer formulation (molecular weight, protection level), exposure (dose, NILS), PEB (PAG/quencher loading, PEB time), and development (developer concentration, polymer hydrophilicity).

3.1 *Polymer Formulation*

Figures 3(a) and 3(b) quantify the particle generation for a resist polymer as a function of degree of polymerization and composition. The results indicate that the volume percentage of insoluble particles decreases with increasing polymer molecular weight. The higher molecular weight enhances the extent of chain entanglement in the polymer matrix and the increased entanglement makes the erosion phenomenon less probable, thereby producing fewer insoluble particles. Figure 3(b) shows that the particle generation first increases and then decreases with an increase in the initial protection level of the polymer. The further the polymer composition is from the solubility switch protection level, the higher the possibility is of finding an insoluble volume in the solubility crossover region. The solubility switch for APEX resists occurs below 30% protection level under normal development conditions, so there is an increase in particle generation as protection level initially increases above 30%. However, the particle generation process depends not only on the existence of an insoluble volume but also on the existence of a connected pathway of soluble material surrounding the particle to "erode" the particle from the bulk. The further increase in the protection level reduces the developer penetration significantly and thus suppresses particle generation. Therefore, there exists a range of protection levels where the particle generation is at a maximum. Ideally, the resist should be formulated with a polymer protection level outside of that range, depending on other process constraints.

3.2 *Exposure*

Figures 4(a) and 4(b) show the particle formation as a function of the NILS of the aerial image and the exposure dose. An aerial image with a higher NILS produces a steeper chemical gradient, narrowing the solubility switch crossover region, which results in a lower insoluble particle generation. The higher dose increases the acid concentration and

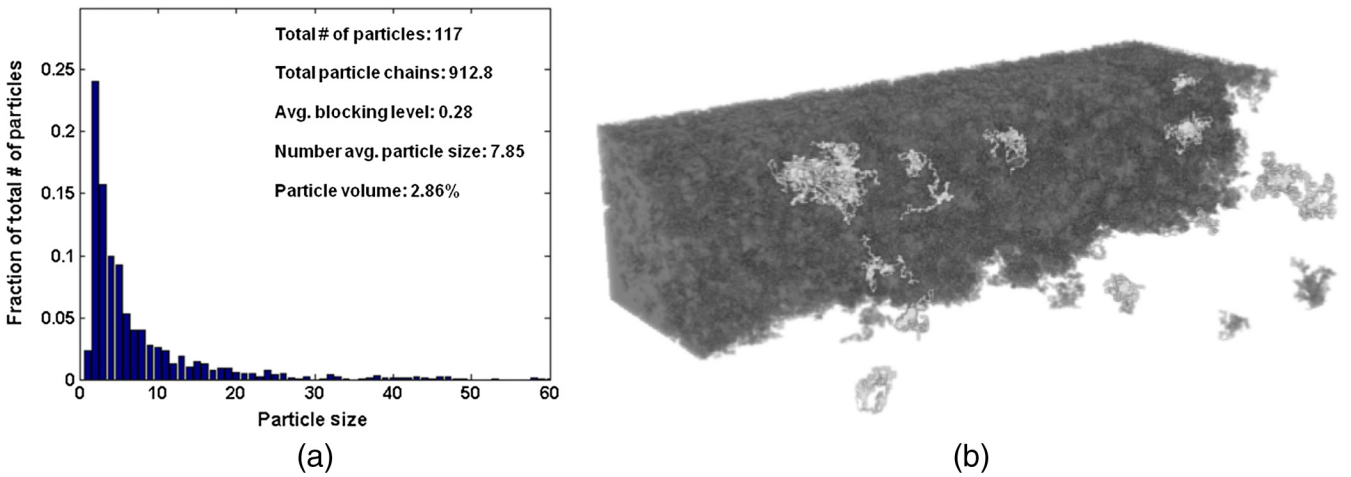

Fig. 2 (a) Particle size distribution for a typical simulation case (average of 10 runs), where the number of polymer chains corresponds to the particle size. Also shown is the postanalysis data that can be obtained after the simulation run. (b) A snapshot of one of the simulation runs showing the insoluble particles generated during the photoresist dissolution.

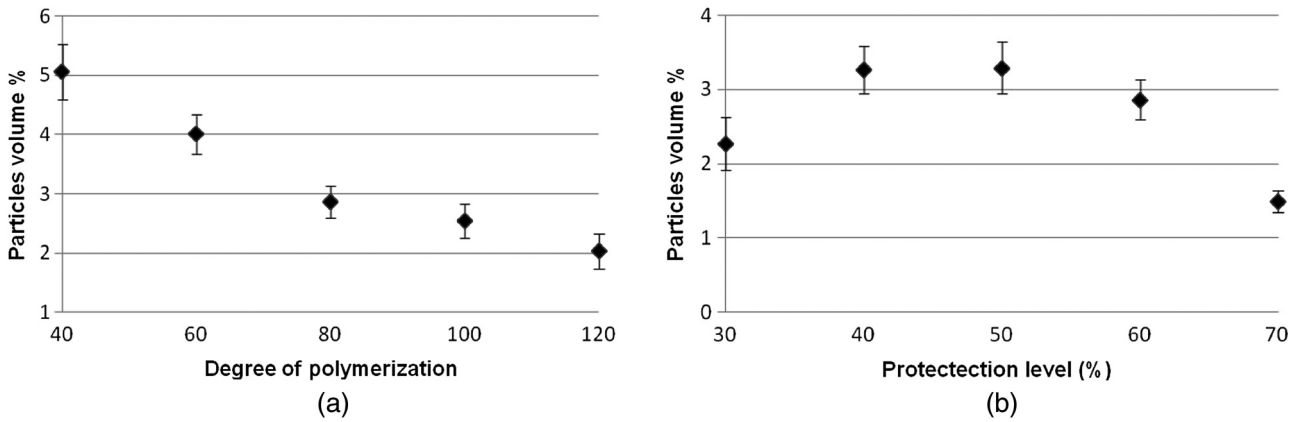

Fig. 3 Particle volume percentage as a function of (a) degree of polymerization and (b) initial protection level of the polymer. In each case, the dose is varied to get the equal line and space width.

a similar argument holds for the effect of higher PAG loading discussed in the subsequent section. It is worthy to note that unlike other cases, the exposure dose is varied from the dose to size in this case and therefore the feature dimension would vary.

3.3 *Postexposure Bake*

In Figs. 5(a) and 5(b), the percent of particle volume is plotted against PAG and quencher loading. It can be seen that higher PAG and quencher loading minimize the fractional volume of insoluble particles. The higher PAG loading yields higher acid concentration, which improves the chemical gradient and thus reduces the width of the crossover region between completely soluble and insoluble regions (as illustrated in Fig. 6). Likewise adding quencher (base) to the system effectively suppresses the fluctuations in the protection profile near the feature edge. Figure 7 shows the particle volume percentage for different PEB times. The volume

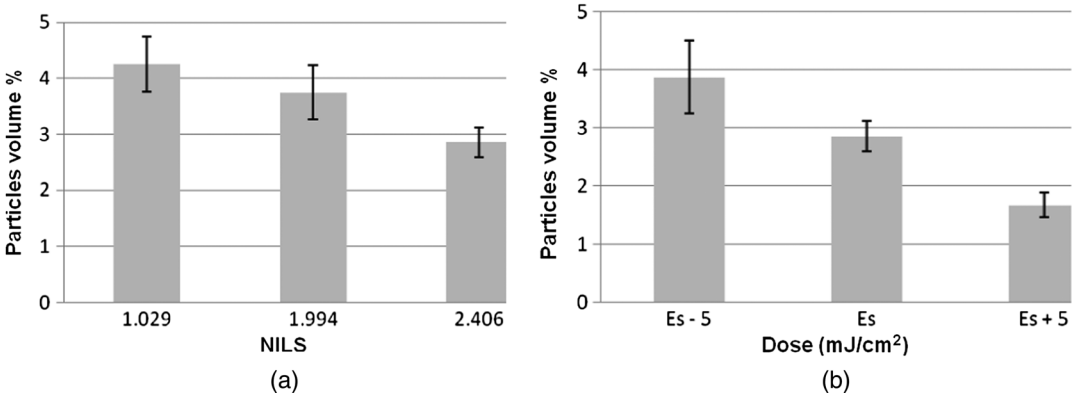

Fig. 4 Particle volume percentage as a function of (a) normalized image log slope (NILS) and (b) exposure dose. Es represents the exposure dose to size. For part (a), the dose is varied to get the equal line and space width in each case.

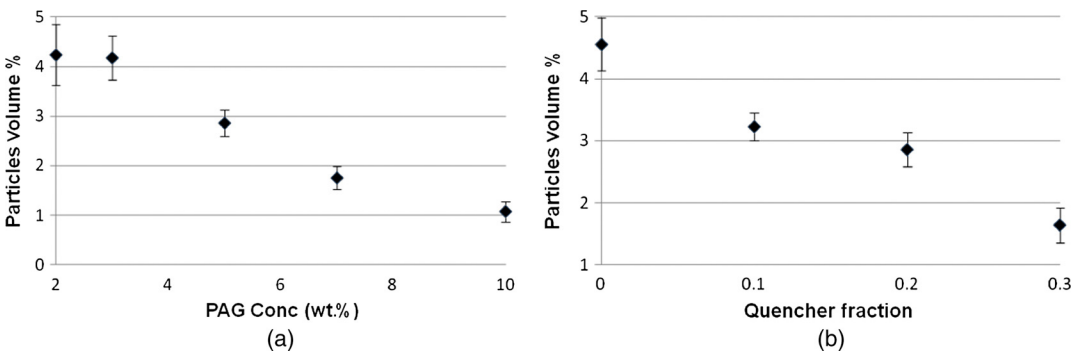

Fig. 5 Particle volume percentage as a function of (a) PAG concentration (wt. % to the polymer) and (b) quencher loading (relative to PAG concentration). In each case, the dose is varied to get the equal line and space width.

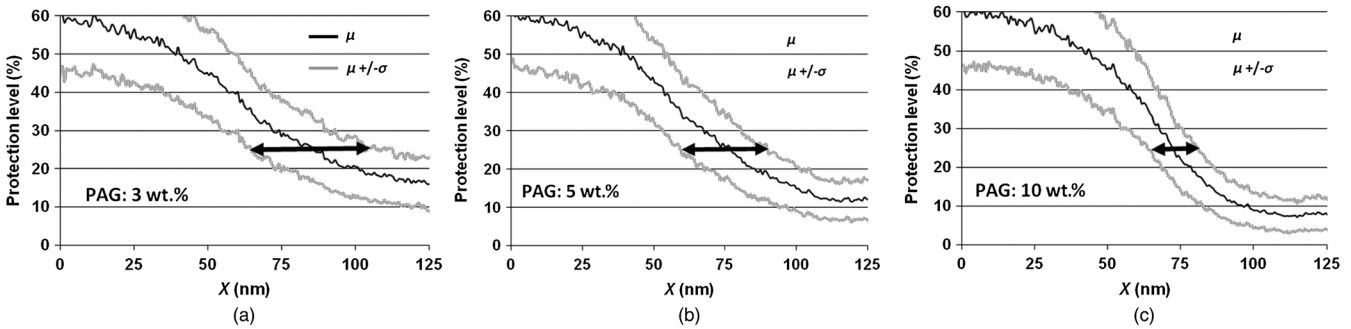

Fig. 6 The chemical gradient in the film for different PAG concentrations (a) 3 wt. %, (b) 5 wt. %, and (c) 10 wt. % illustrating the change in width of the solubility crossover region. The three curves in each figure represent the mean protection level and the limits of one standard deviation in each direction.

percentage of particles first decreases and then increases with an increase in PEB time. This trend suggests that there may be an optimum PEB time that would minimize particle formation.

3.4 *Dissolution*

The exposure and PEB process conditions directly affect the chemical gradient and consequently the particle generation phenomenon. Given the chemical gradient profile in the exposed film, the dissolution process can be altered to minimize particle generation during the photoresist dissolution. Figures 8(a) and 8(b) illustrate the effect of parameters related to the important photoresist dissolution step on particle generation. Increasing the developer concentration and the increment in hydrophilicity of polymer components (unprotected/protected part of the polymer chain) serves to suppress particle generation. The higher developer concentration increases a favorable interaction between the developer and the ionized part of the polymer chain. Hence, the more concentrated developer is able to solvate chains/particles with higher protection levels, which would have been insoluble otherwise. This also means that the water rinse step may be a source of particle generation due to the sudden reduction in pH of the solution and precipitation of material that is soluble in the developer.

The increase in the hydrophilicity of the polymer or a reduction in interfacial energy between the developer and the polymer components also results in higher chain/particle solvation and a corresponding reduction in particle generation. The impact of resist surface properties on particle formation can help to guide material design. For example, lactones are incorporated in 193-nm resists to increase the polarity of very hydrophobic alicyclic polymers.[18] Based on the observations presented above, this would also be

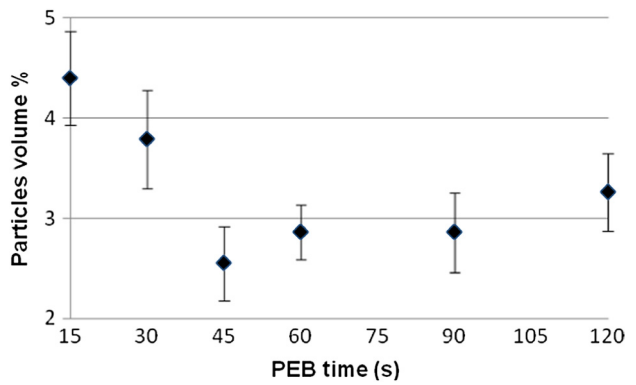

Fig. 7 Particle volume percentage as a function of postexposure bake (PEB) time. The dose is varied to get the equal line and space width in each case.

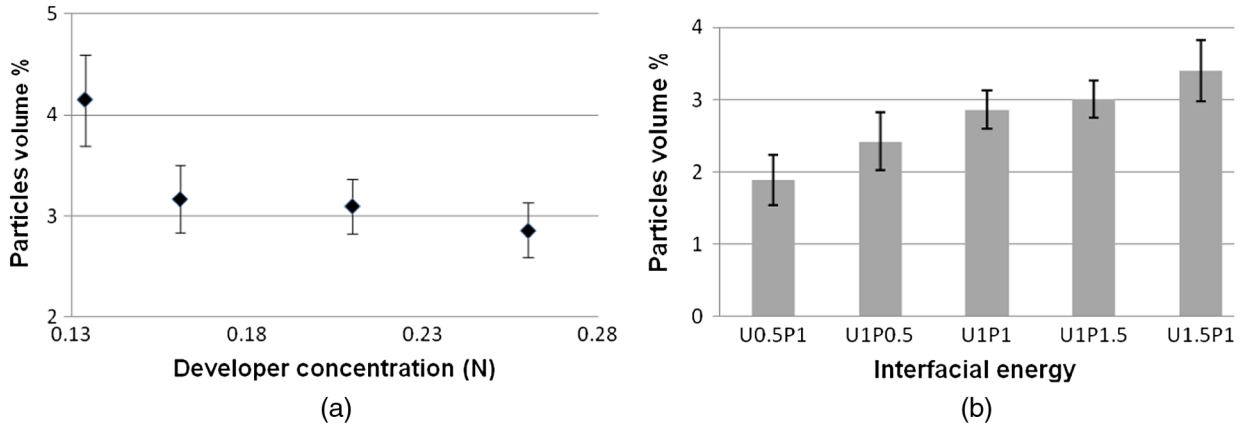

Fig. 8 Particle volume percentage as a function of (a) developer concentration and (b) the interfacial energy of polymer components with the developer. U and P represent the unprotected and the protected parts of the polymer, where UmPn would mean that the interfacial energies of the unprotected and the protected parts are increased *m* and *n* times, respectively. In each case, the dose is varied to get the equal line and space width.

expected to assist in suppressing the particle generation. However, increased hydrophilicity may result in polymer swelling and poor patterning due to the low solubility contrast. Therefore, the optimal hydrophilicity of polymer components is, like most things in resist design, a trade-off.

4 Line Edge Roughness

LER characterization using only the standard deviation of the line edge neglects the spatial distribution of roughness along the edge. The quantification of the spectral aspects of LER requires the set of three parameters, namely sigma value σ, correlation length L_c, and roughness exponent α. The sigma value is the standard deviation of the line edge and commonly reported as LER. The correlation length represents the length scale after which the line edges are uncorrelated. Also, the roughness exponent is indicative of the relative contribution of high-frequency fluctuations to LER. The lower the value of roughness exponent, the higher the contribution from high-frequency fluctuations. The power spectral density (PSD) function is generally employed to examine the frequency content of roughness and is the edge variance per unit spatial frequency. Mathematically, it is evaluated as the square of the modulus of the Fourier transform of the line edge divided by the normalization factor equal (or proportional) to the length of the measured line. Figure 9 shows a schematic plot of the PSD function. It shows that the distribution of the magnitude of LER variance as a function of spatial frequency with the area under the PSD curve equals the square of the sigma value. The correlation length corresponds to the frequency around which the PSD curve has the onset of the downward slope. For the length scale higher than the correlation length, i.e., in the low-frequency region, the random noise is uncorrelated. However below the correlation length L_c, i.e., at higher frequencies, the roughness is correlated and the slope of the PSD curve is dependent on the roughness exponent. The following function can be used to fit the PSD curve to extract the relevant parameters:

$$\frac{\mathrm{psd}(f)}{\mathrm{psd}(0)} = \frac{1}{1 + (2\pi \cdot f L_c)^{1+2\alpha}} + B, \tag{1}$$

where f is the spatial frequency and B is added to account for any white noise.[19–25] The roughness sigma value can be obtained either by determining the area under the PSD curve or directly evaluating the standard deviation of the line edge. Different mechanisms contribute to the formation

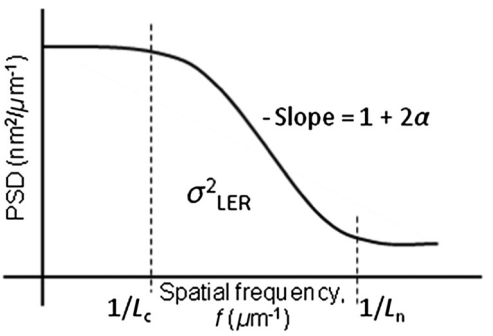

Fig. 9 Schematic plot of PSD function for line-edge roughness illustrating the characterization parameters, namely sigma value σ, correlation length L_c, and roughness exponent α.

of LER, including inhomogeneity of the resist components, illumination optics, reaction coupled diffusion during PEB, and polymer dissolution. In principle, each mechanism should have a different LER response and the PSD analysis could be used to assess the relative contribution of different lithographic steps in low-/high-frequency domain. It is worthy to note that in the current study, LER reflects the edge roughness only from the prospective of lithographic steps. Subsequent steps, like etch, may have been shown to have an effect on LER, correlation length, and roughness exponent.[26]

A film of APEX type resist with dimensions of 65× 500 × 100 nm [X-, Y-, Z-dimensions in Fig. 10(a)] was simulated using a $92 \times 712 \times 144$ lattice structure with periodic boundary conditions in X- and Y-directions. The choice of the dimensions is directed to capture the low-frequency aspects of LER in Y-dimension. The resist that was simulated is formulated from a polymer with degree of polymerization of 80, pKa of 10.25, and 5 t. % PAG loading. The PEB time and the temperature were 60 s and 90°C, respectively. A development time of 15 s with standard 0.26 N developer concentration was used in the development step. Any patterned line after the dissolution step would have a sidewall angle depending on the various processing steps involved. The calculation of LER is therefore highly dependent on the choice of the XY plane for determining the line edge. Therefore, an open frame development is used in the dissolution step and the roughness is evaluated as the film thickness variation in the Z-direction along the Y-direction at different X values. Figure 10(b) shows the film thickness variation roughness along the Y-direction at three X values. The final PSD curve reported is an average of PSD curves obtained at different X values from 20 simulation runs. In addition to PEB and the development step, the aerial and resist image profile also affects the LER. To eliminate any contribution from the optics to the roughness, a step profile of an acid concentration is used in the PEB step. Any PAG within the given top section of the film is converted to acid, effectively simulating the exposure with NILS equals to infinity.

4.1 *Dissolution*

This section examines the characteristics of the roughness due to the dissolution of homopolymer (unprotected or partially protected). Figures 11(a) and 11(b) show the PSD curves and fitted parameters of roughness due to the dissolution of unprotected polymer for the different dissolution times depicting the dynamic behavior of roughness. One can see that the roughness sigma value (area under the PSD curve) rapidly increases as the time progresses and the roughness increases in the entire (low/high) frequency domain. Also, the correlation length increases fast with time as shown by the left shift of the onset frequency for correlated roughness in Fig. 11(a). Both the roughness and the correlation length finally saturate in ~1 s and do not show much increase after that. However, this saturation could be the artifact of the finite length of the line (500 nm in this case) simulated. The length of the line examined should be more than six to 10 times the correlation length to get the stable roughness sigma value.[27] After the initial growth, the roughness exponent remains similar, implying that

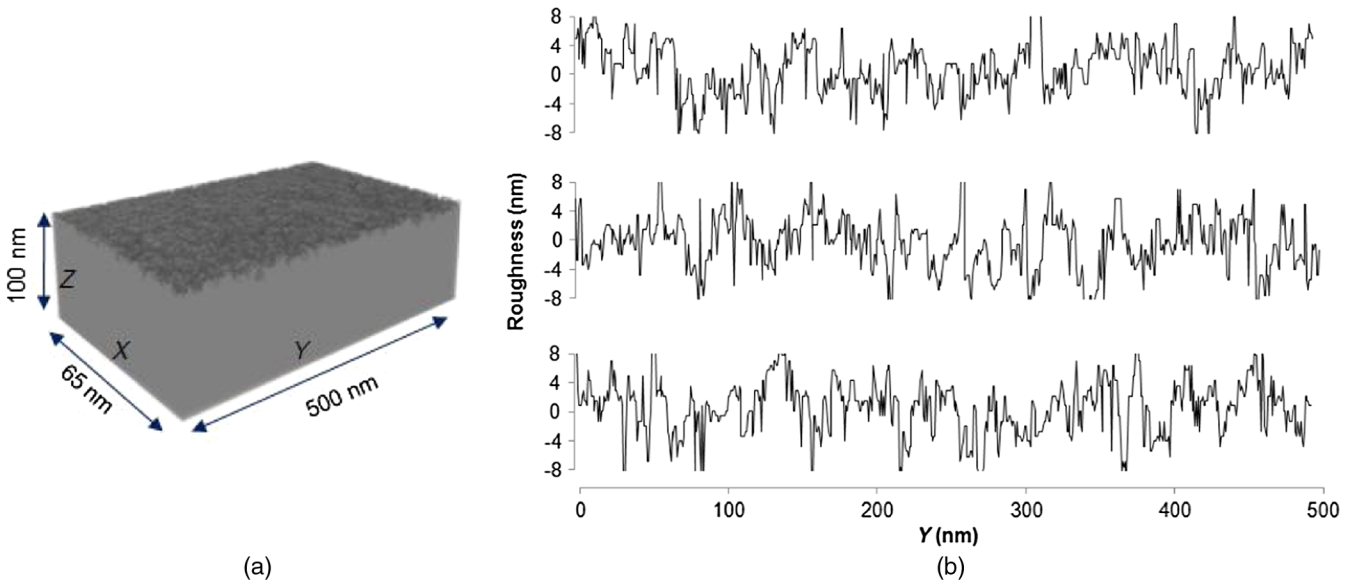

Fig. 10 (a) Simulated film configuration and (b) film thickness variations along *Y*-direction for three different *X* values.

the underlying mechanism of roughness formation remains unchanged with time for uniform polymer configuration.

Figure 12 shows the PSD curves and fitted parameters of roughness due to the dissolution of 10% protected polymers of different molecular weights. The roughness increases with the polymer molecular weight throughout the frequency domain. On the other hand, the roughness exponent for the dissolution process remains similar for different polymer molecular weights. Similar analysis for the roughness due to the dissolution of polymers with protection level ranging from 0% to 15% has shown the same behavior, i.e., the roughness sigma value increases with an increase in protection level but the roughness exponent remains similar.

4.2 *PEB and Dissolution*

This section examines the characteristics of the roughness of polymer with both the PEB and the dissolution as the underlying mechanisms for roughness formation. Unlike the previous section, the inclusion of PEB step results in non-uniform polymer protection level with the film depth. Figures 13(a) and 13(b) show the PSD curves and the fitted parameters of roughness for polymers of different molecular weights when both PEB and subsequent dissolution steps are taken into account. There are several distinctions that can be pointed out when comparing Fig. 13 with earlier Fig. 12 where only polymer dissolution is considered. First, there is a considerable reduction in correlation length as seen by the right shift of the onset frequency for correlated roughness shown by the arrow pointing right. Second, unlike the case with only polymer dissolution, here the roughness exponent decreases with the increase in polymer molecular weight. Third, the roughness sigma value does not vary much with the change in polymer molecular weight. The dependency of roughness exponent on the polymer molecular weight results in crossing of PSD curves at a certain

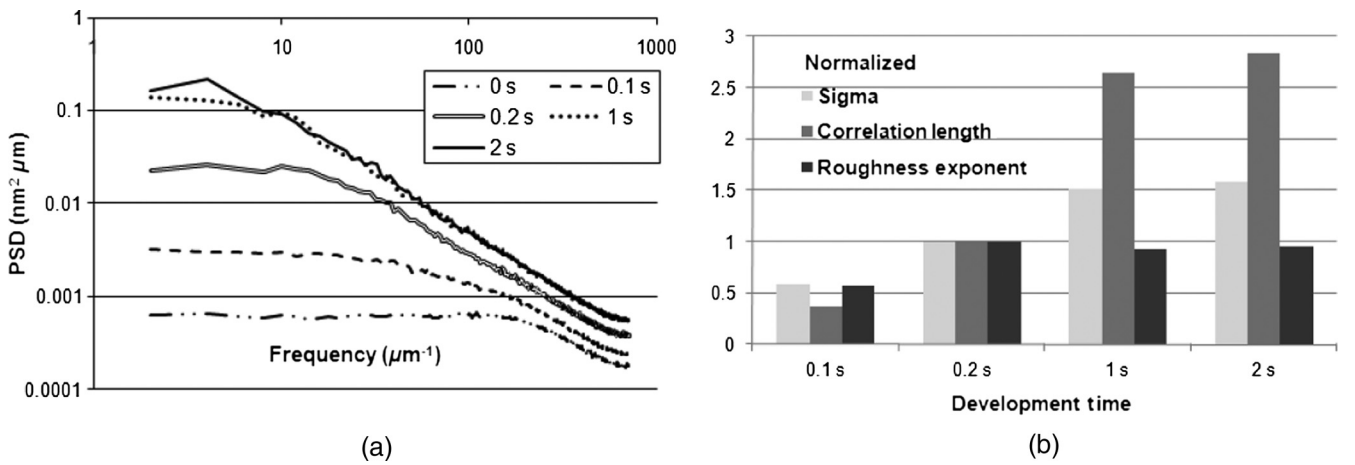

Fig. 11 (a) PSD curves and (b) fitted parameters of roughness (sigma value, correlation length, and roughness exponent) of unprotected polymer for the different dissolution times. The sigma, the correlation length, and the roughness exponent are normalized with the values at 0.2 s dissolution time, i.e., 1.7 nm, 5.4 nm, and 0.28, respectively.

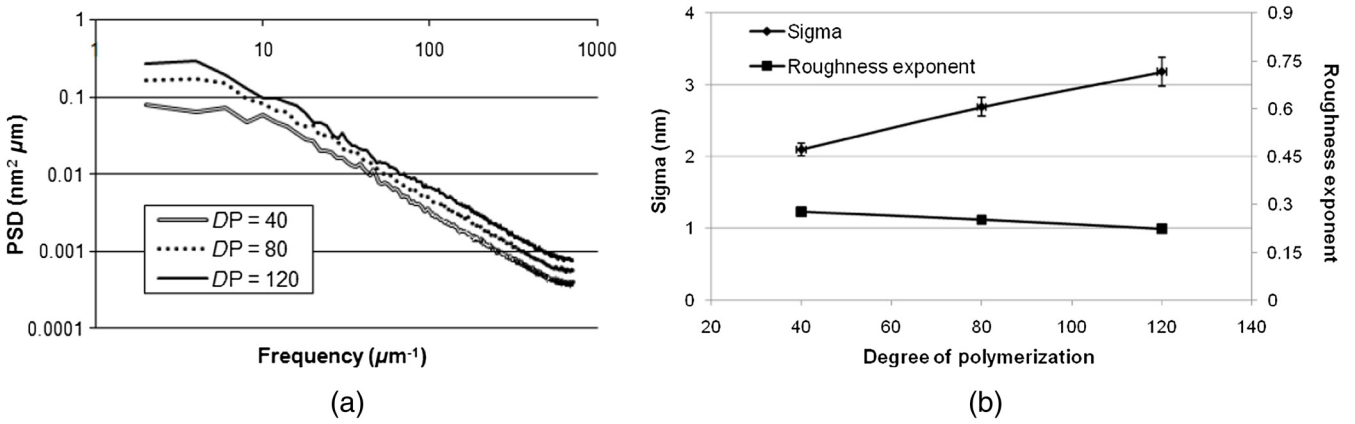

Fig. 12 (a) PSD curves and (b) fitted parameters (sigma value and roughness exponent) of roughness due to the dissolution of 10% protected polymers of different molecular weights.

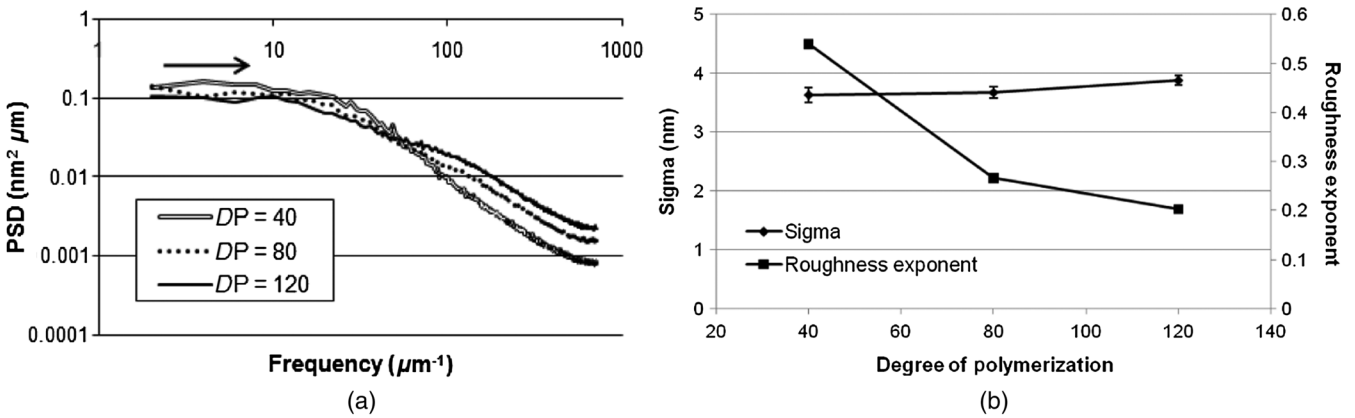

Fig. 13 (a) PSD curves and (b) the fitted parameters of roughness for polymers of different molecular weights after the PEB and the dissolution step.

crossover frequency. This crossover results in different contributions to roughness in low-/high-frequency domain for different polymer molecular weights. In the low-frequency region (left of the crossover frequency region), the polymer with the lower molecular weight has higher roughness sigma value, while in the high-frequency region (right of the crossover frequency region), the polymer with the higher molecular weight has higher roughness sigma value. The net result is that the overall sigma value of the roughness accounting for all frequencies is not strongly dependent on the polymer molecular weight when PEB and dissolution both are considered.

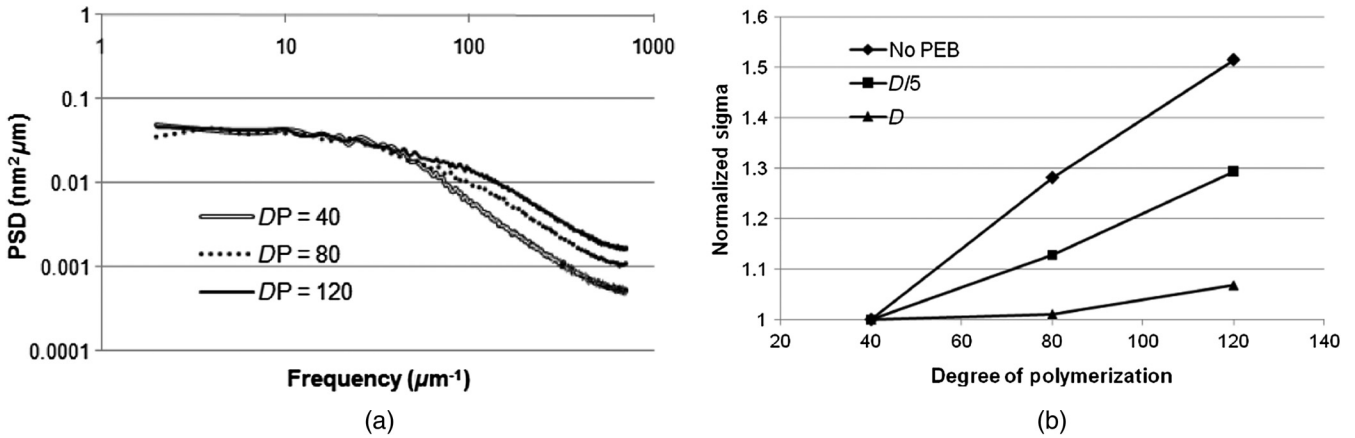

Fig. 14 (a) PSD curves of polymers with different molecular weights for reduced acid diffusivity, $D/5$. (b) The roughness sigma value responses for different molecular weight polymers for the three cases considered above, i.e., no PEB in Fig. 12(a), PEB with acid diffusivity $D/5$ and D in Figs. 14(a) and 13(a). The sigma values in each case are normalized with the values for the polymer with degree of polymerization of 40, i.e., 2.1, 2.4, and 3.6 nm, respectively.

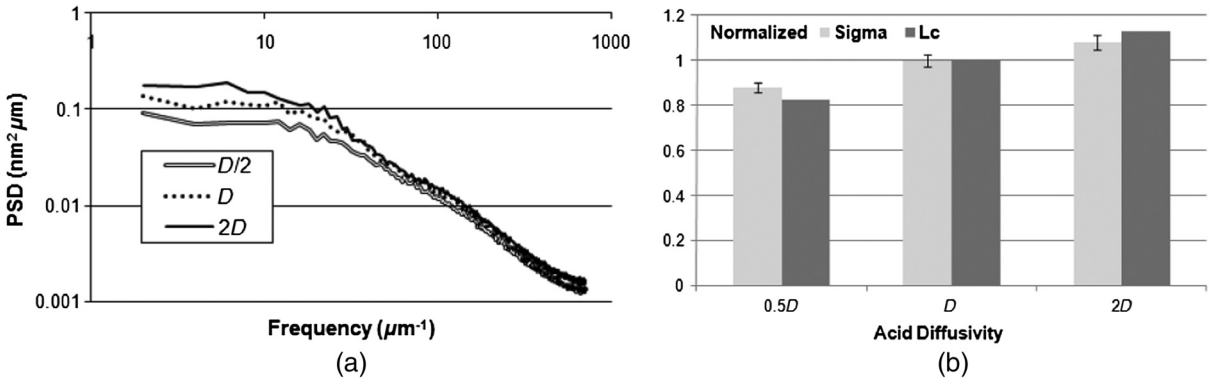

Fig. 15 (a) PSD curves and (b) the fitted parameters of roughness (sigma value and correlation length) for different amounts of acid diffusions during the PEB. The sigma and the correlation length are normalized with the values at normal acid diffusivity (*D*), i.e., 3.7 and 7.2 nm, respectively.

The difference in the two cases compared in Figs. 12(a) and 13(a) is due to the different roughness responses to the polymer molecular weights in low-frequency region. In the high-frequency region, the higher molecular weight polymer has higher sigma value in both the cases and therefore one can argue that the dissolution is the dominant mechanism in high-frequency region and the dissolution results in a lower roughness sigma value with smaller polymer size or radius of gyration. On the other hand, the different roughness responses in the low-frequency region due to the introduction of PEB in the latter case suggests that the underlying noise due to the acid diffusion during PEB is the dominant contributor to the low-frequency roughness and it is the PEB that results in higher roughness sigma at the lower polymer molecular weights.

Polymer dissolution (without PEB) can be considered as the extreme case of polymer dissolution (with PEB) as the acid diffusion approaches zero. Therefore, the roughness response to the polymer molecular weight could be controlled by altering the acid diffusion. Figure 14(a) shows the PSD curves of polymers with the different molecular weights for reduced acid diffusivity. The reduction in acid diffusion results in the molecular weight response with the negligible difference in the low-frequency region and the similar response as observed for earlier cases in the high-frequency domain. Figure 14(b) summarizes the roughness sigma value response for different molecular weight polymers for different cases considered above in Figs. 12(a), 13(a), and 14(a). The sensitivity of roughness sigma value to polymer molecular weight is the most for the purely dissolution case. However, as the acid diffusion increases, the roughness sigma value becomes less sensitive to polymer molecular weight for the range of diffusivities examined in the current study. This analysis suggests that the role of polymer molecular weight with respect to the LER is contingent on the extent of acid diffusion. At low acid diffusion, the dominant mechanism for LER generation is dissolution and lower polymer molecular weight would result in lower LER. With higher acid diffusion and PEB as the dominant mechanism, the lower polymer molecular weight produces the same or even higher LER. This result could be particularly relevant to the molecular glass community," where significant effort has been focused on the use of lower molecular weight polymer materials as a means to reduce LER.

The other commonly proposed measures for reducing LER, namely low acid diffusivity and the use of quenchers, were assessed (keeping the polymer molecular weight constant at a degree of polymerization of 80). Figures 15(a) and 15(b) show the PSD curves and the fitted parameters of roughness for different amount of acid diffusions. The

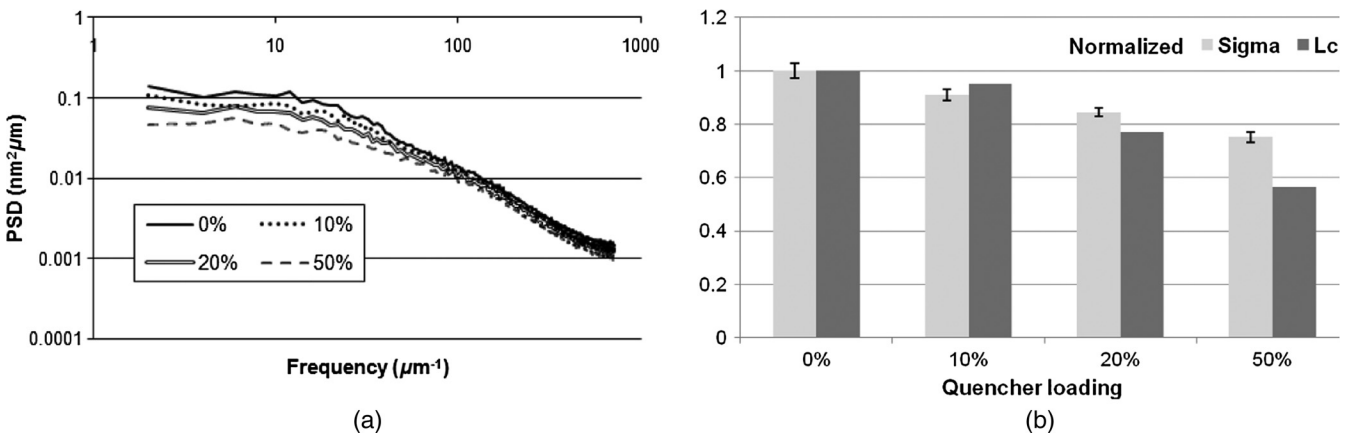

Fig. 16 (a) PSD curves and (b) the fitted parameters of roughness (sigma value and correlation length) quantifying the effect of quencher loading (relative to PAG moles) on the roughness. The sigma and the correlation length are normalized with the values at 0% quencher loading, i.e., 3.7 and 7.2 nm, respectively.

roughness sigma value decreases with the lower acid diffusion and the reduction mainly occurs in low frequency. Also, the correlation length decreases with the lower acid diffusion. Figures 16(a) and 16(b) show the PSD curves and the fitted parameters of roughness quantifying the effect of adding quenchers on the roughness. Similar to lower acid diffusivity, the addition of quenchers also reduces the roughness sigma value predominantly in the low-frequency region. The correlation length shows the same trend. These observations further support the claim that the underlying noise due to the PEB step mainly contributes to low-frequency roughness.

5 Conclusions

A mesoscale model has been adapted to study particle generation during photoresist dissolution. New PEB and dissolution models have been incorporated that allow exploration of statistical excursions in the development path due to variance around the mean protection level. Particles are generated during photoresist dissolution when there is a connected pathway of soluble material that envelops a volume an insoluble material. An extensive parametric study was done to assess the extent of particle generation as a function of polymer formulation (molecular weight, protection level), exposure (dose, NILS), PEB (PAG/quencher loading, PEB time), and development (developer concentration, polymer hydrophilicity). The relative contributions of the PEB and the dissolution steps to LER in the low-/high-frequency domain have also been investigated. Dissolution predominantly affects the high-frequency roughness while the PEB has the greatest impact on LER in the low-frequency domain. The commonly proposed measures to reduce LER such as the use of low molecular weight polymers, addition of quenchers, varying acid diffusion length, etc., were assessed. This study can provide a means to guide material design and optimize process conditions to minimize particle generation and LER.

Acknowledgments

The authors wish to thank the Tokyo Electron Limited (TEL) for funding this work; Texas Advanced Computing Center (TACC) at the University of Texas at Austin for providing computing resources; DuPont for generous donations of materials; Dr. Vishwanath H. Dalvi and the Willson Research Group for advice and useful discussions.

References

1. G. M. Schmid, "Understanding molecular scale effects during photoresist processing," Ph.D. Thesis, University of Texas, Austin (2003).
2. J. E. Meiring et al., "Using mesoscale simulation to explore photoresist line edge roughness," *Proc. SPIE* **5753**, 350–360 (2005).
3. International Technology Roadmap for Semiconductors (ITRS) official website, http://www.itrs.net/.
4. J.-Y. Lee et al., "Effect of line edge roughness (LER) and line width roughness (LWR) on sub-100 nm device performance," *Proc. SPIE* **5376**, 426–433 (2004).
5. Y. Ma, H. J. Levinson, and T. Wallow, "Line edge roughness impact on critical dimension variation," *Proc. SPIE* **6518**, 651824 (2007).
6. M. Carcasi et al., "Extension of 248 nm Monte Carlo, mesoscale models to 193 nm platforms," *Proc. SPIE* **7639**, 76392K (2010).
7. S. Chauhan et al., "Polymer dissolution model: an energy adaptation of the critical ionization theory," *Proc. SPIE* **7273**, 727336 (2009).
8. M. D. Stewart, "Catalyst diffusion in positive-tone chemically amplified photoresists, Ph.D. Thesis, University of Texas, Austin (2003).
9. S. V. Postnikov, "Transport properties of photogenerated acid and silylating agent in polymer films," Ph.D. Thesis, University of Texas, Austin (1999).
10. A. Reiser et al., "The molecular mechanism of novolak-diazonaphthoquinone resists," *Eur. Polym. J.* **38**(4), 619–629 (2002).
11. M. N. Ozisik, *Heat Conduction*, 3rd ed., Wiley (1993).
12. G. M. Schmid et al., "Electrostatic effects during dissolution of positive tone photoresists," *J. Vac. Sci. Technol., B* **20**(6), 2913–2919 (2002).
13. P. C. Tsiartas et al., "Mechanism of phenolic polymer dissolution," *Macromolecules* **30**(16), 4656–4664 (1997).
14. L. W. Flanagin et al., "Probabilistic model for the mechanism of phenolic polymer dissolution," *Proc. SPIE* **3333**, 268–277 (1998).
15. M. E. Colburn, "Step and flash imprint lithography: a low-pressure, room-temperature nanoimprint lithography," Ph.D. Thesis, University of Texas, Austin (2001).
16. C. J. Van Oss, R. J. Good, and M. K. Chaudhury, "Additive and nonadditive surface tension components and the interpretation of contact angles," *Langmuir* **4**(4), 884–891 (1988).
17. J. N. Israelachvili, *Intermolecular and Surface Forces: With Applications to Colloidal and Biological Systems*, p. 296, Academic Press, London (1985).
18. H. Ito, H. D. Truong, and P. J. Brock, "Lactones in 193 nm resists: what do they do?," *Proc. SPIE* **6923**, 692318 (2008).
19. C. Mack, "Stochastic modeling in lithography: autocorrelation behavior of catalytic reaction-diffusion systems," *J. Micro/Nanolithogr., MEMS, MOEMS* **8**(2), 029701 (2009).
20. C. Mack, "Stochastic modeling in lithography: use of dynamical scaling in photoresist development," *J. Micro/Nanolithogr., MEMS, MOEMS* **8**(3), 033001 (2009).
21. W. G. Lawrence, "Spatial frequency analysis of line edge roughness in nine chemically related photoresists," *Proc. SPIE* **5039**, 713–724 (2003).
22. A. Philippou, T. Mülders, and E. Schöll, "Impact of photoresist composition and polymer chain length on line edge roughness probed with a stochastic simulator," *J. Micro/Nanolithogr., MEMS, MOEMS* **6**(4), 043005 (2007).
23. A. Pawloski et al., "Line edge roughness and intrinsic bias for two methacrylate polymer resist systems," *J. Microlithogr., Microfabr., Microsyst.* **5**(2), 023001 (2006).
24. V. Constantoudis et al., "Line edge roughness and critical dimension variation: fractal characterization and comparison using model functions," *J. Vac. Sci. Technol., B* **22**(4), 1974–1981 (2004).
25. G. Lorusso et al., "Spectral analysis of line width roughness and its application to immersion lithography," *J. Microlithogr., Microfabr., Microsyst.* **5**(3), 033003 (2006).
26. V. Constantoudis et al., "Line-edge-roughness transfer during plasma etching: modeling approaches and comparison with experimental results," *J. Micro/Nanolithogr., MEMS, MOEMS* **8**(4), 043004 (2009).
27. V. Constantoudis, G. Patsis, and E. Gogolides, "Photoresist line-edge roughness analysis using scaling concepts," *J. Microlithogr. Microfabr., Microsyst.* **3**, 429–435 (2004).

Siddharth Chauhan received his BTech in chemical engineering from IIT Kanpur, India, in 2005 and PhD in chemical engineering from the University of Texas at Austin in 2010. He joined Intel Corporation in 2011 in Assembly and Test Technology Development and is currently a member of Computational Lithography Technology.

Mark Somervell received his BChE in chemical engineering from the Georgia Institute of Technology in 1996 and his MS and PhD from the University of Texas at Austin in 1998 and 2000, respectively. He worked as a member of technical staff in the Silicon Technology Development Group for Texas Instruments and now works as a member of technical staff within the Advanced Technology Group at Tokyo Electron America.

Michael Carcasi received his BS in chemical engineering from the University of Texas at Austin in 1997. He joined Tokyo Electron in 1998. He is currently a senior research scientist in Tokyo Electron's Advanced Technology Group.

Steven Scheer received his BS in chemical engineering from the Missouri University of Science and Technology in 1997 and MS and PhD in chemical engineering from the University of Texas at Austin in 2001 and 2002, respectively. He worked at IBM Microelectronics from 2002 to 2005, then he joined Tokyo Electron Ltd. and formed the Lithography Advanced Technology Group based in Austin, Texas.

Roger T. Bonnecaze received his BS in chemical engineering from Cornell University in 1985 and his MS and PhD from the California Institute of Technology in 1987 and 1991, respectively. He served as a postdoctoral research fellow at the University of Cambridge from 1991 to 1992. He joined the faculty of the Department of Chemical Engineering at the University of Texas at Austin in 1998.

Chris A. Mack received his BS in physics, chemistry, electrical, and chemical engineering from Rose-Hulman Institute of Technology in 1982, his MS in electrical engineering from the University of Maryland in 1989, and his PhD in chemical engineering from the University of Texas at Austin in 1998. After working in FINLE Technologies and KLA-Tencor, he currently writes, teaches, and consults in the field of semiconductor lithography.

C. Grant Willson received his BS and PhD in organic chemistry from the University of California at Berkeley and his MS in organic chemistry from San Diego State University. He joined the faculties of the Departments of Chemical Engineering and Chemistry at the University of Texas at Austin in 1993 after holding a position as an IBM fellow and manager of the Polymer Science and Technology area at the IBM Almaden Research Center in San Jose, California.